

University of Louisville

ThinkIR: The University of Louisville's Institutional Repository

Faculty Scholarship

6-1-2021

Predicting the Spectrum of UGC 2885, Rubin's Galaxy with Machine Learning

Benne Holwerda

University of Louisville, benne.holwerda@louisville.edu

John F. Wu

William C. Keel

Jason Young

Ren Mullins

See next page for additional authors

Follow this and additional works at: <https://ir.library.louisville.edu/faculty>



Part of the [Astrophysics and Astronomy Commons](#)

Original Publication Information

Benne W. Holwerda *et al.* "Predicting the Spectrum of UGC 2885, Rubin's Galaxy with Machine Learning." 2021 *Astrophysical Journal* 914(2): 1-6.

ThinkIR Citation

Holwerda, Benne; Wu, John F.; Keel, William C.; Young, Jason; Mullins, Ren; Hinz, Joannah; Ford, K. E. Saavik; Barnby, Pauline; Chandar, Rupali; Bailin, Jeremy; Peek, Josh; Pickering, Tim; and Böker, Torsten, "Predicting the Spectrum of UGC 2885, Rubin's Galaxy with Machine Learning" (2021). *Faculty Scholarship*. 833.

<https://ir.library.louisville.edu/faculty/833>

This Article is brought to you for free and open access by ThinkIR: The University of Louisville's Institutional Repository. It has been accepted for inclusion in Faculty Scholarship by an authorized administrator of ThinkIR: The University of Louisville's Institutional Repository. For more information, please contact thinkir@louisville.edu.

Authors

Benne Holwerda, John F. Wu, William C. Keel, Jason Young, Ren Mullins, Joannah Hinz, K. E. Saavik Ford, Pauline Barmby, Rupali Chandar, Jeremy Bailin, Josh Peek, Tim Pickering, and Torsten Böker



Predicting the Spectrum of UGC 2885, Rubin’s Galaxy with Machine Learning

Benne W. Holwerda¹, John F. Wu², William C. Keel³, Jason Young⁴, Ren Mullins¹, Joannah Hinz^{5,6},
K. E. Saavik Ford^{7,8,9,10}, Pauline Barmby¹¹, Rupali Chandar¹², Jeremy Bailin³, Josh Peek^{2,13}, Tim Pickering^{5,6}, and
Torsten Böker¹⁴

¹ Physics & Astronomy Department, University of Louisville, Louisville, KY 40292, USA; benne.holwerda@louisville.edu

² Space Telescope Science Institute, 3700 San Martin Drive, Baltimore, MD 21219, USA

³ Department of Physics and Astronomy, University of Alabama Box 870324, Tuscaloosa, AL 35487-0324, USA

⁴ Mount Holyoke College, 50 College Street, South Hadley, MA 01075, USA

⁵ Steward Observatory, University of Arizona, 933 North Cherry Avenue, Tucson, AZ 85721-0065, USA

⁶ MMT Observatory, P.O. Box 210065, Tucson, AZ 85721-0065, USA

⁷ Dept. of Science, Borough of Manhattan Community College, City University of New York, New York, NY 10007, USA

⁸ Dept. of Astrophysics, American Museum of Natural History, New York, NY 10024, USA

⁹ Physics Program, CUNY Graduate Center, City University of New York, New York, NY 10016, USA

¹⁰ Center for Computational Astrophysics, Flatiron Institute, New York, NY 10010, USA

¹¹ Department of Physics & Astronomy, Institute for Earth & Space Exploration, University of Western Ontario, 1151 Richmond Street, London, Ontario, Canada

¹² Department of Physics & Astronomy, The University of Toledo, Toledo, OH 43606, USA

¹³ Department of Physics & Astronomy, Johns Hopkins University, Baltimore, MD 21218, USA

¹⁴ European Space Agency, c/o STScI, 3700 San Martin Drive, Baltimore, MD 21219, USA

Received 2021 February 10; revised 2021 May 6; accepted 2021 May 7; published 2021 June 25

Abstract

Wu & Peek predict SDSS-quality spectra based on Pan-STARRS broadband *grizy* images using machine learning (ML). In this article, we test their prediction for a unique object, UGC 2885 (“Rubin’s galaxy”), the largest and most massive, isolated disk galaxy in the local universe ($D < 100$ Mpc). After obtaining the ML predicted spectrum, we compare it to all existing spectroscopic information that is comparable to an SDSS spectrum of the central region: two archival spectra, one extracted from the VIRUS-P observations of this galaxy, and a new, targeted MMT/Binospec observation. Agreement is qualitatively good, though the ML prediction prefers line ratios slightly more toward those of an active galactic nucleus (AGN), compared to archival and VIRUS-P observed values. The MMT/Binospec nuclear spectrum unequivocally shows strong emission lines except $H\beta$, the ratios of which are consistent with AGN activity. The ML approach to galaxy spectra may be a viable way to identify AGN supplementing NIR colors. How such a massive disk galaxy ($M^* = 10^{11} M_\odot$), which uncharacteristically shows no sign of interaction or mergers, manages to fuel its central AGN remains to be investigated.

Unified Astronomy Thesaurus concepts: [Giant galaxies \(652\)](#); [Galaxy nuclei \(609\)](#); [Disk galaxies \(391\)](#)

1. Introduction

In recent years, astronomical machine learning (ML) has transformed from a niche subject to a well-developed suite of accessible and interpretable algorithms. ML algorithms are used for catalogs, time series, imaging, and unstructured data across a wide array of astronomy subdisciplines (e.g., exoplanets, Shallue & Vanderburg 2018; radio interferometry, Vafaei Sadr et al. 2020; transient photometry, Villar et al. 2020; and studies of the interstellar medium, Xu et al. 2020). For extragalactic imaging data, ML is regularly relied upon for classifying galaxy morphology (e.g., Dieleman et al. 2015; Beck et al. 2018), quantifying observed properties (e.g., Smith et al. 2021), and predicting spectroscopic properties (e.g., Pasquet et al. 2019; Wu & Boada 2019). These advances have enabled ML to take on an outsized role in mitigating the observational disparity between enormous survey imaging data sets and limited spectroscopic follow-up campaigns (e.g., Wu & Peek 2020). While ML results are robust for estimating the properties of typical galaxies, it is less clear if predictions are reliable for rare or unusual systems.

Spectroscopy surveys lag behind imaging ones in coverage and depth simply because of the longer integration time per object (see Davies et al. 2018; Driver et al. 2019, for a discussion on ongoing and near-future surveys). Predicting

spectra or spectral features based on imaging is therefore a worthwhile endeavor for both scientific and planning purposes.

UGC 2885 (“Rubin’s Galaxy”) is the largest and most massive spiral galaxy ($R_p = 38.1$ kpc, $M_* = 2.2 \times 10^{11} M_\odot$) in the local universe (Rubin 1980). It shows very regular rotation with a maximum rotation velocity of 298 km s^{-1} ($M_{\text{tot}} = 1.50 \times 10^{12} M_\odot$; Rubin et al. 1980; Roelfsema & Allen 1985; Wiegert & English 2014; McGaugh & Schombert 2015), rising from the center, indicating a substantial and extended dark matter halo (Marr 2015). The galaxy has star formation throughout its disk (Hunter et al. 2013), four spiral arms, and a specific incidence of globular clusters that hints at an uneventful accretion history (B. W. Holwerda et al. 2021, in preparation). It lies just outside the Sloan Digital Sky Survey’s footprint and has no SDSS or DES spectra.

UGC 2885 defies easy classification: to the first order it is an Sc galaxy but it is at the outermost edge of the mass and size envelope for its class. The initial identification of UGC 2885 as the largest isolated spiral galaxy by Rubin (1980) was confirmed by Romanishin (1983) for the whole Uppsala Galaxy Catalog. We measure the Petrosian radius of Rubin’s galaxy at 38.1 kpc (97”) in *sdss-r*. Ogle et al. (2016, 2019) introduce “Super spirals,” a class of massive disk galaxies at the utmost top of the stellar mass-star formation rate ($M_*\text{-SFR}$) relation. Ogle et al. (2016) note that “Super spirals” are almost

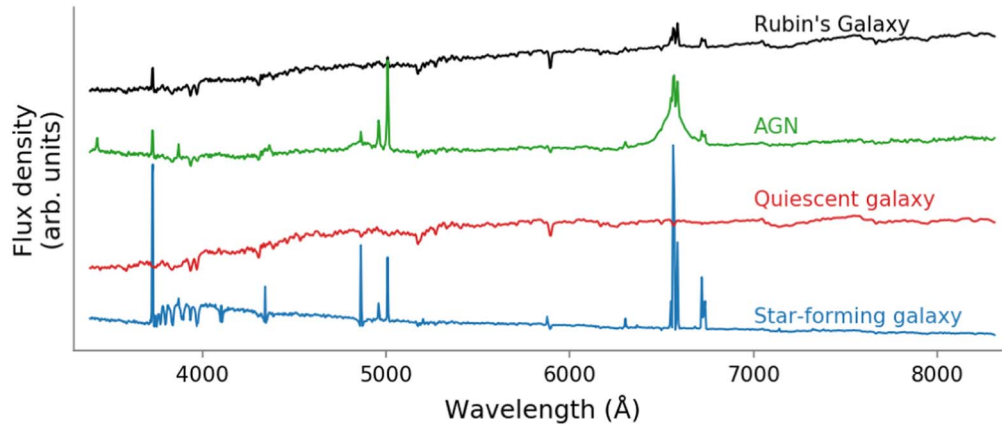


Figure 1. The prediction by the ML method of Wu & Peek (2020) for Rubin’s galaxy (top) and reference SDSS spectra for an example of an AGN, a quiescent galaxy, and a star-forming galaxy, all shifted to the rest frame. The spectral features of Rubin’s galaxy fall between those of a quiescent and an AGN-dominated galaxy.

never in an isolated environment and often show signs of a recent interaction, e.g., perturbed morphology, dual nuclei, or other signs of significant merger activity. Rubin’s galaxy does not meet these qualifications as it has a lower SFR and does not show signs of recent interaction, which appear to be typical for this class of galaxies. Saburova et al. (2021) discusses giant low surface brightness (LSB) disk galaxies. Once again, UGC 2885 does not meet those specifications either: its star formation is too high and concentrated in a more typical brightness disk. These giant LSB galaxies also often seem to be visibly disturbed from recent accretion or merger activity. Yet Rubin’s galaxy is remarkably unperturbed.

A $\sim 10^{11} M_{\odot}$ stellar mass galaxy typically has an active galactic nucleus (AGN) and our question for this study is: is Rubin’s galaxy exceptional here as well? Keel (1983a) remains the only study to attempt to characterize the nucleus of this galaxy and does not reach a firm conclusion. Does UGC 2885 show signs of an active nucleus? One would expect its spectrum to lie in the categories of LINER or star formation/AGN mix. Can this be predicted from broadband photometry using ML? How good is the ML prediction of this galaxy’s spectrum? As a local extreme of size and mass, the lack of an SDSS spectrum offered the opportunity for a direct test of this prediction.

The purpose of this paper is to report a “closed envelope” test of the ML predicted spectrum for the center of Rubin’s galaxy from Wu & Peek (2020) and compare it to spectra obtained from private archives and recent observations: the prediction was made first and then compared to spectra of comparable quality.

2. Machine-learning Prediction of Rubin’s Galaxy’s Spectrum

We generate the predicted spectrum for Rubin’s galaxy using the method described in Wu & Peek (2020). Briefly, the method uses a convolutional neural network (CNN), trained on $56'' \times 56''$ *grizy* image cutouts of galaxies from the Pan-STARRS 3π Steradian Survey DR2, and predicts the galaxies’ optical spectra ($3''$ aperture, SDSS resolution, and signal-to-noise ratio (S/N)). Galaxy spectra are normalized, shifted to a common reference frame, and rebinned in 1000 logarithmically spaced elements. A variational autoencoder represents each spectrum using six latent variables, which can be robustly “decoded” back into SDSS spectra (Portillo et al. 2020). Wu &

Peek (2020) train a CNN to predict galaxies’ SDSS spectra solely using image cutouts. Figure 1 shows the results of this ML approach applied to the Pan-STARRS image of Rubin’s galaxy. In the comparisons this spectrum is shifted to the galaxy redshift of $v = 5802 \text{ km s}^{-1}$ (Canzian et al. 1993).

3. Data

To verify the ML prediction, we obtained two archival spectra, extracted one from the VIRUS-P IFU observation, and obtained new MMT/Binospec observations. The apertures used in each observation are shown in Figure 2.

The first comparison spectrum is originally from Keel (1983a, 1983b), who conducted an aperture spectroscopic survey of nearby galaxies to search for AGN activity. Keel (1983a) reported line strengths for $H\alpha$, $[N \text{ II}]$, and $[S \text{ II}]$. Their verdict on nuclear activity was inconclusive.

Archival data is a scan of a $4''.7$ diameter circular aperture spectrum from the Mount Lemmon 1.5 m (60 inch) telescope taken on 1981 February 4/5, shown in the top panel in Figure 3, and a $6''.1$ circular aperture spectrum taken using the Intensified Image Dissector Scanner on the KPNO 2.1 m, shown in the second panel in Figure 3. The archival spectra are normalized by the maximum value in the spectrum for ease of comparison to the ML spectrum. The 60 inch spectrum closely resembles an SDSS spectrum in aperture and S/N but is limited in wavelength coverage. The KPNO spectrum has a similar wavelength coverage but much lower S/N and a wider aperture compared to SDSS spectra.

Recent VIRUS-P IFU observations of Rubin’s galaxy seek to reveal star formation and abundances (J. Young et al. 2021, in preparation). A blue spectrum ($< 5800 \text{ \AA}$) was extracted using a $4''.16$ aperture to compare with the ML prediction, shown in Figure 3, third panel.

A targeted $3 \times 300 \text{ s}$ optical spectrum was obtained at the MMT Observatory with the instrument Binospec (Fabricant et al. 2019) in 2020 November with a position angle = 35° using the 270 lines mm^{-1} grating with a central wavelength of 6500 \AA . The observations were taken at R.A. = 3:53:02.4811, decl. = +35:35:22.103 with a $1''$ slit. Data reduction was completed by the Binospec automated pipeline, which is an open-source IDL software package distributed under the

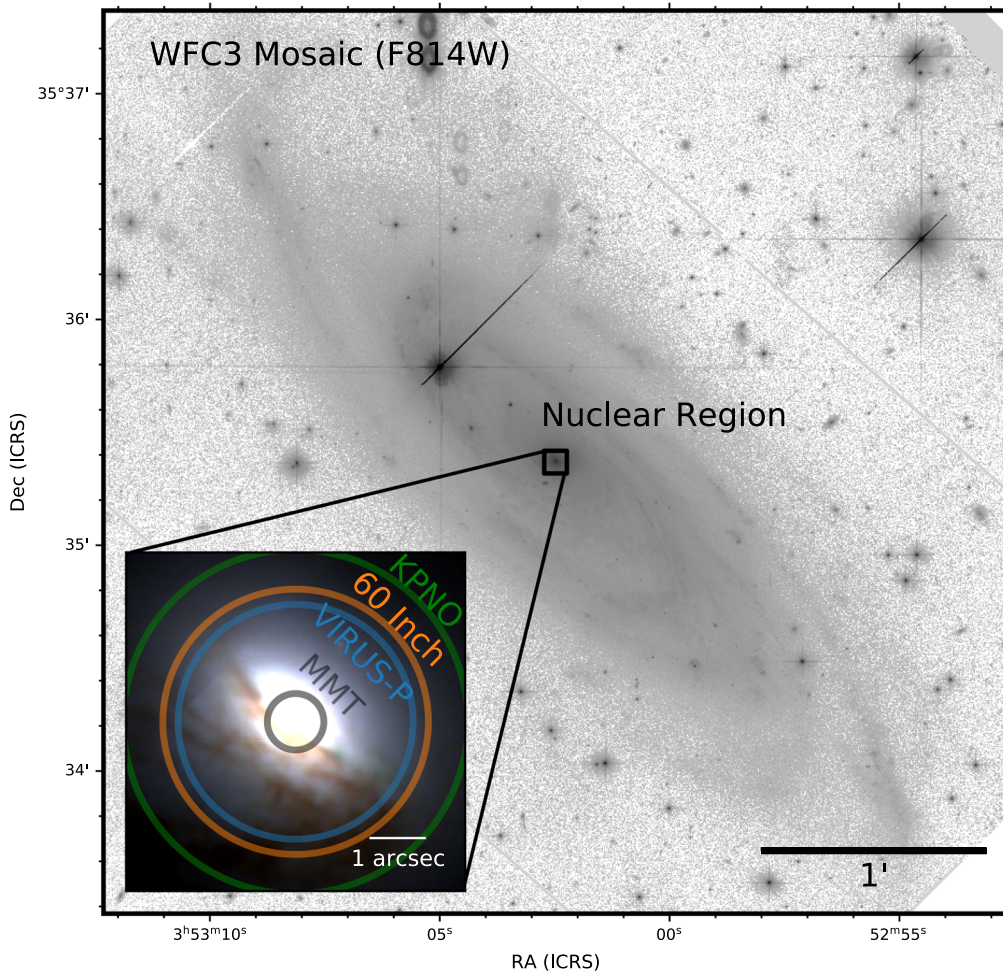


Figure 2. The nucleus of Rubin’s galaxy from the larger HST mosaic. A clear dustlane partially obscures the central stellar cluster. The inset shows the apertures of the spectroscopic observations, which are marked using the same color scheme as in Figure 3: Mount Lemon 60 inch (orange), 2.1 KPNO (green), VIRUS-P (blue), and MMT (white for contrast).

GPLv3 license (Chilingarian et al. 2019).¹⁵ This standard reduction resulted in the spectrum in Figure 3, fourth panel.

Both the VIRUS-P and the MMT/Binospec spectra have been renormalized using the maximum value in each spectrum’s bandpass (VIRUS-P 4000–5700 Å and MMT 4000–7000 Å). This leaves a gradual difference in continuum between normalized ML and either spectrum. Subsequently, we modeled this continuum difference between the ML prediction and the observed spectrum as a third degree polynomial to remove bandwidth-wide effects. We subtracted this continuum difference to facilitate a direct comparison between spectra and their features in Figure 3.

4. Discussion

4.1. How Well Did ML Perform?

Figure 3 shows excellent agreement between the ML predicted spectrum and the observations. Discrepancies in the stellar continuum are easily attributed to night sky lines (present in the 60 inch spectrum <6800 Å but not preserved in the SDSS vectorization). In the residual, one can identify a slight gradient in the KPNO spectrum’s continuum (<5000 Å),

which is a similar calibration difference. Discrepancies in $H\alpha$ /[N II] and [O III] line strengths are notable in Figure 3.

The 60 inch and VIRUS-P spectra have closely comparable but not identical apertures to SDSS ($\sim 4''$ and $3''$ diameters, respectively, Figure 2), and a slight offset is to be expected. Both archival spectra (Figure 3, top two panels) show excellent agreement with the ML predicted spectrum within their respective noise levels. The major differences are telluric features (e.g., 6800 Å in the 60 inch spectrum in Figure 3), not included in the original ML prediction (telluric features are a source of noise in the training set, and are therefore left out as much as practical).

The VIRUS-P spectrum broadly agrees well with the ML prediction. The only deviations are the [O III] emission line and the He I absorption, which are both slightly underpredicted by the ML method (Figure 3, third panel). About a third of the equivalent width in the [O III] emission and the He I absorption is missing (Figure 3, bottom panel).

The MMT/Binospec spectrum (Figure 3, fourth panel) focuses on the very central region of Rubin’s galaxy. The [O III] and $H\alpha$ /[N II] emission line strengths, as well as the [S II] absorption features at 4000 Å, do appear to be underpredicted by the ML in comparison to the MMT spectrum.

There are two factors resulting in differences between the ML predicted spectra and those observed: the aperture of the

¹⁵ https://bitbucket.org/chil_sai/binospec

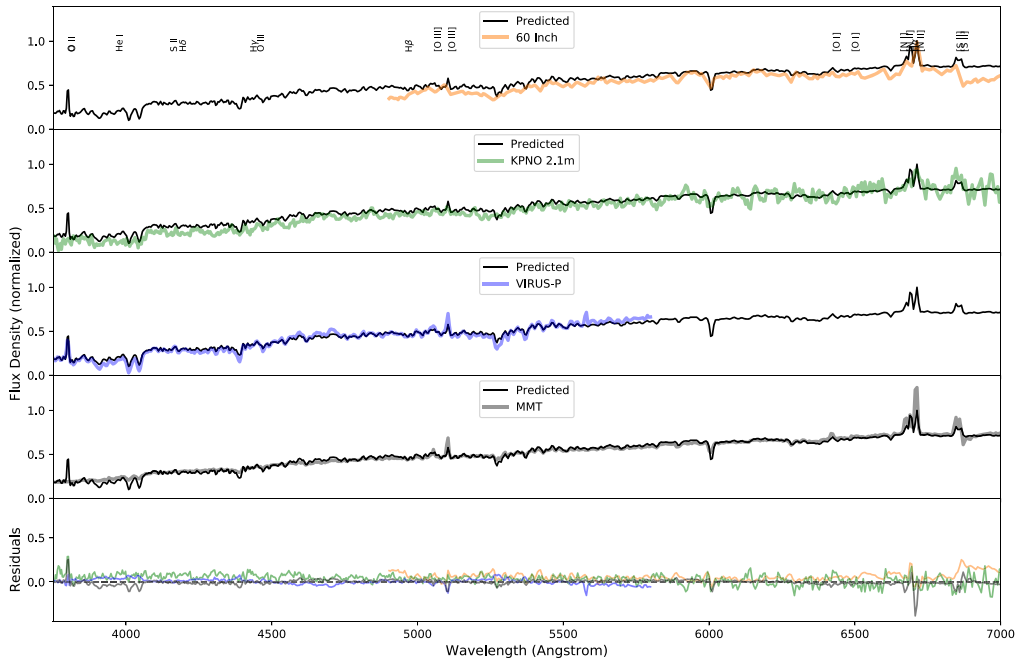


Figure 3. The ML predicted spectrum (black line in the top four panels) and the observed spectra, from Keel (1983a) using the Mount Lemon 60 inch (top panel, orange), the KPNO 2.1 m telescope (second panel, green), from the VIRUS-P IFU instrument (third panel, blue), and the 2020 MMT Binospec observation (bottom panel, gray). The bottom panel shows the residuals of each spectrum and the ML prediction.

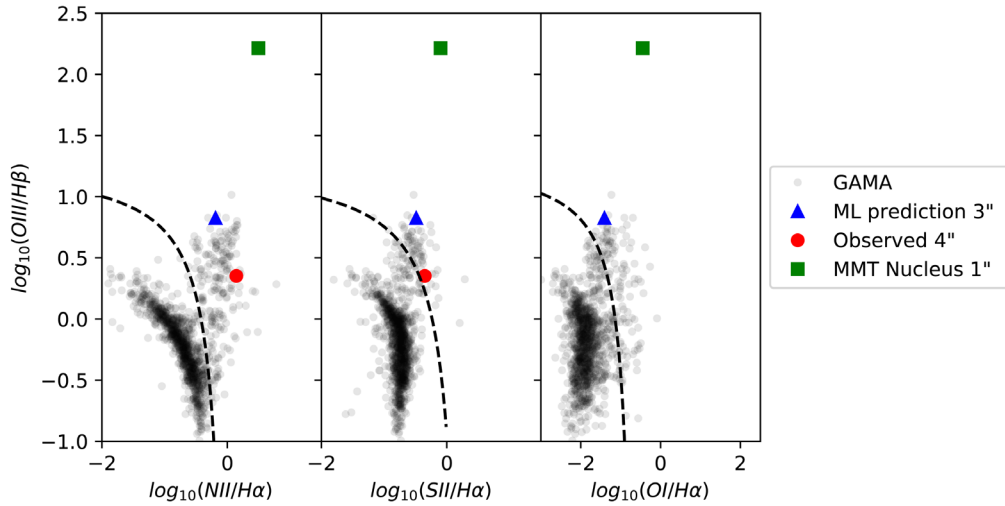


Figure 4. The BPT diagnostic diagram for nuclear activity. The Galaxy And Mass Assembly Survey data is shown for comparison with the Kauffmann et al. (2003) star formation/AGN demarcation (dashed lines). The observed line strengths reported in Keel (1983a) and the VIRUS-P observations for Rubin’s galaxy put it in the active galaxies category. The ML predicted spectrum puts it in the AGN category. None of the line ratios prefer LINER or Seyfert classifications (Kewley et al. 2006). The MMT line ratios are complicated as $H\beta$ is not well constrained, skewing the vertical position of the nucleus on the y-axis.

observed spectra and the aperture-distance effects in the SDSS training sample.

Figure 2 illustrates that the archival spectra and VIRUS-P are for a slightly larger aperture and the MMT one for a smaller aperture than an SDSS spectrum on this galaxy would have been. Stronger $H\beta$ and $[O III]$ from the nucleus can be explained by less dilution of the AGN signal. This can be seen as the progression of stronger observed emission lines in Figure 3 with smaller apertures.

Second, the ML algorithm was trained on SDSS with a known aperture-distance effect (dilution of AGN signal in more distant galaxies), matching the spectra of more distant galaxies to Rubin’s Galaxy’s nucleus with a wider aperture diluting the AGN signal.

4.2. AGN?

Identifying lower-power AGN can be difficult because selection effects are the most notable at the lower luminosities. Traditionally, one would select obscured or low-power AGN from IR colors rather than X-ray or emission lines in spectra. The ML approach offers an alternative, with Rubin’s galaxy being an instructive example of one that could be identified using imaging alone.

Figure 4 shows where the observed and the ML predicted line strengths place the nucleus of Rubin’s galaxy on the BPT diagram (Baldwin et al. 1981). The line strengths implied by the ML predicted spectrum imply strongly that Rubin’s galaxy is an AGN (blue triangle in Figure 4).

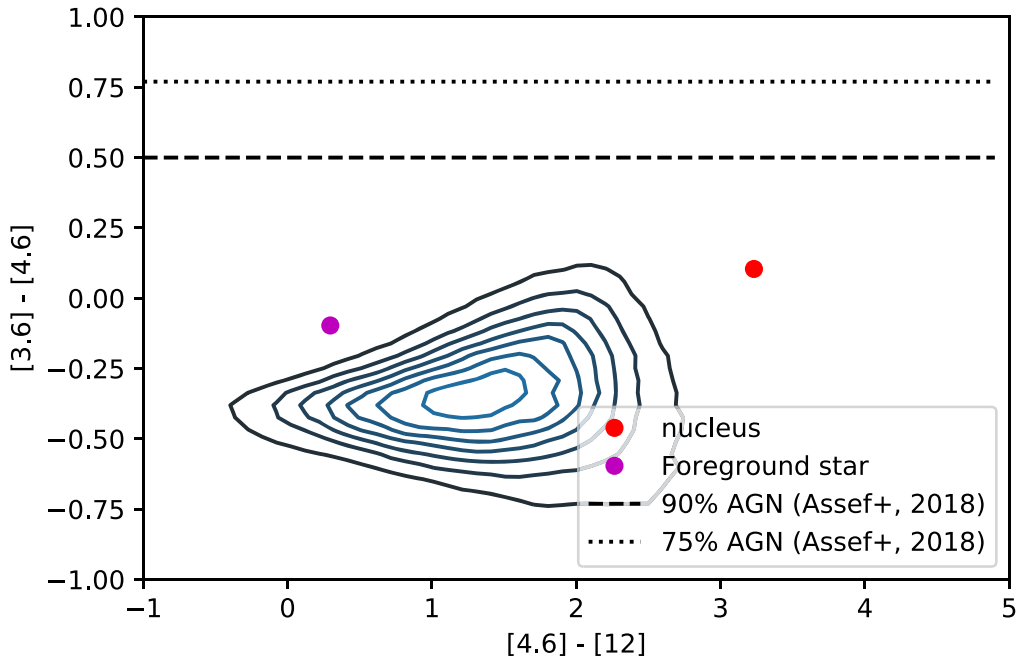


Figure 5. WISE colors of sources in the GAMA Equatorial Fields (Cluver et al. 2014). The WISE colors of the ALLWISE catalog sources at the position of Rubin’s galaxy are shown. The colors of the bright foreground star projected on the disk of UGC 2885 are as would be expected. The colors of the nucleus are located away from the bulk of normal galaxies (contours) but the $[4.6]-[3.6]$ color does not quite reach the AGN criterion of Assef et al. (2018).

A combination of Keel (1983a) and VIRUS-P line strengths are more consistent with a lower-power AGN, closer to the dividing line between active galaxies and star-forming galaxies (red circle in Figure 4). The MMT/Binospec line strengths put the nucleus of Rubin’s galaxy solidly in the AGN category (green square in Figure 4). The MMT spectrum does not constrain the $H\beta$ well and this skews the $O\text{ III}/H\beta$ ratio. The observed or predicted line ratios are not consistent with those of either a LINER or Seyfert according to the Kewley et al. (2006) criteria.

Figure 5 shows the WISE colors of the central region of Rubin’s galaxy for comparison with the classifications of Jarrett et al. (2011) and Cluver et al. (2014). The WISE colors are consistent with those of spiral, star-forming disk galaxies. The source catalog entry corresponding to the center of Rubin’s Galaxy is in the part of color-space where star-forming galaxies border on obscured AGN and Seyfert galaxies, according to Figure 5 in Cluver et al. (2014). However the WISE $[3.6]-[4.5]$ color criterion from Assef et al. (2016, 2018) does not place Rubin’s galaxy in the AGN bracket (dashed lines in Figure 5). Given the angular resolution of WISE, dilution of the AGN signal by the PSF likely accounts for this lack of AGN identification, i.e., the WISE flux is dominated by the stellar population of Rubin’s galaxy. Based on the spectroscopic line strengths, the center of Rubin’s galaxy is indeed an AGN. WISE colors have the benefit of suffering less from dust obscuration allowing for unbiased searches of AGN in the nearby universe. However, the WISE color selection still misses AGN such as these and the ML approach may be a way to fill in the missing population.

4.3. Discussion

It is exciting to see that the ML prediction of an SDSS-quality spectrum of this galaxy is so reliable, even when this galaxy resides in the space between star-forming and AGN. The ML method outperforms WISE color selection, the

preferred method of identifying AGN in objects without a spectrum. A successful ML prediction in the loci of galaxy populations is reassuring but a tangible success for an extreme object is especially encouraging. How the ML algorithm transfers from, e.g., Pan-STARRS broadband *grizy* images to the Rubin Observatory’s LSST looks to be a promising example of transfer learning in astronomy.

The combined line strengths of Rubin’s Galaxy point to ongoing AGN activity. Combined with the very extended star-forming disk, the presence of an AGN makes this galaxy an interesting case: a massive disk galaxy, with no signs of interaction, relatively normal star formation activity, and very regular rotation, yet using secular mechanisms only to fuel its central source.

5. Conclusions

The ML predicted SDSS-quality spectrum from Wu & Peek (2020) is remarkably close to the observed spectra (Figure 3). Deviations can be attributed to small differences in aperture or to residuals from telluric lines. The emission lines in the ML prediction are underpredicting the $[O\text{ III}]$ and $H\alpha$ and $[N\text{ II}]$ doublet compared to $[O\text{ II}]$. The successful identification of this galaxy’s spectrum is a promising development in the use of ML. It is an encouraging development for future use on the Rubin Observatory data.











In order to supply gas to the central black hole, the gas must lose angular momentum, and astronomers have long suspected that galaxy collisions (or at least interactions) provide the requisite torque to bring that gas into the nucleus (e.g., Hong et al. 2015; Dietrich et al. 2018; Gao et al. 2020; Marian et al. 2020). However, interactions are not the only avenue for fueling the AGN (e.g., McKernan et al. 2010; Marian et al. 2019). Rubin’s galaxy is an example of an extremely isolated, undisturbed, and massive galaxy that shows clear evidence of nuclear activity, and it may prove a useful laboratory to study the secular fueling processes on a grand scale. Further

dissection of the inner regions of the galaxy may shed light on the secular mechanisms that supply fuel to AGN.

The authors would like to thank the anonymous referee for the effort and time spent improving the manuscript. Observations reported here were obtained at the MMT Observatory, a joint facility of the University of Arizona and the Smithsonian Institution. Support for this work was provided by NASA through grant No. GO-15107 from the Space Telescope Science Institute, which is operated by AURA, Inc., under NASA contract NAS 5-26555.

Software: Astropy (Astropy Collaboration et al. 2013).

ORCID iDs

Benne W. Holwerda  <https://orcid.org/0000-0002-4884-6756>
 John F. Wu  <https://orcid.org/0000-0002-5077-881X>
 William C. Keel  <https://orcid.org/0000-0002-6131-9539>
 Ren Mullins  <https://orcid.org/0000-0001-7044-0632>
 Joannah Hinz  <https://orcid.org/0000-0003-3339-0546>
 Pauline Barmby  <https://orcid.org/0000-0003-2767-0090>
 Rupali Chandar  <https://orcid.org/0000-0003-0085-4623>
 Jeremy Bailin  <https://orcid.org/0000-0001-6380-010X>
 Josh Peek  <https://orcid.org/0000-0003-4797-7030>
 Torsten Böker  <https://orcid.org/0000-0002-5666-7782>

References

- Assef, R. J., Stern, D., Noirot, G., et al. 2018, *ApJS*, 234, 23
 Assef, R. J., Walton, D. J., Brightman, M., et al. 2016, *ApJ*, 819, 111
 Astropy Collaboration, Robitaille, T. P., & Tollerud, E. J. 2013, *A&A*, 558, A33
 Baldwin, J. A., Phillips, M. M., & Terlevich, R. 1981, *PASP*, 93, 5
 Beck, M. R., Scarlata, C., Fortson, L. F., et al. 2018, *MNRAS*, 476, 5516
 Canzian, B., Allen, R. J., & Tilanus, R. P. J. 1993, *ApJ*, 406, 457
 Chilingarian, I., Moran, S., Paegert, M., et al. 2019, in ASP Conf. Ser. 523, *Astronomical Data Analysis Software and Systems XXVII*, ed. P. J. Teuben et al. (San Francisco, CA: ASP), 629
 Cluver, M. E., Jarrett, T. H., Hopkins, A. M., et al. 2014, *ApJ*, 782, 90
 Davies, L. J. M., Robotham, A. S. G., Driver, S. P., et al. 2018, *MNRAS*, 480, 768
 Dieleman, S., Willett, K. W., & Dambre, J. 2015, *MNRAS*, 450, 1441
 Dietrich, J., Weiner, A. S., Ashby, M. L. N., et al. 2018, *MNRAS*, 480, 3562
 Driver, S. P., Liske, J., Davies, L. J. M., et al. 2019, *MNRAS*, 487, 46
 Fabricant, D., Fata, R., Epps, H., et al. 2019, *PASP*, 131, 075004
 Gao, F., Wang, L., Pearson, W. J., et al. 2020, *A&A*, 637, A94
 Hong, J., Im, M., Kim, M., & Ho, L. C. 2015, *ApJ*, 804, 34
 Hunter, D. A., Elmegreen, B. G., Rubin, V. C., et al. 2013, *AJ*, 146, 92
 Jarrett, T. H., Cohen, M., Masci, F., et al. 2011, *ApJ*, 735, 112
 Kauffmann, G., Heckman, T. M., White, S. D. M., et al. 2003, *MNRAS*, 341, 33
 Keel, W. C. 1983a, *ApJ*, 269, 466
 Keel, W. C. 1983b, *ApJS*, 52, 229
 Kewley, L. J., Groves, B., Kauffmann, G., & Heckman, T. 2006, *MNRAS*, 372, 961
 Marian, V., Jahnke, K., Andika, I., et al. 2020, *ApJ*, 904, 79
 Marian, V., Jahnke, K., Mechtley, M., et al. 2019, *ApJ*, 882, 141
 Marr, J. H. 2015, *MNRAS*, 453, 2214
 McGaugh, S. S., & Schombert, J. M. 2015, *ApJ*, 802, 18
 McKernan, B., Ford, K. E. S., & Reynolds, C. S. 2010, *MNRAS*, 407, 2399
 Ogle, P. M., Lanz, L., Appleton, P. N., Helou, G., & Mazzarella, J. 2019, *ApJS*, 243, 14
 Ogle, P. M., Lanz, L., Nader, C., & Helou, G. 2016, *ApJ*, 817, 109
 Pasquet, J., Bertin, E., Treyer, M., Arnouts, S., & Fouchez, D. 2019, *A&A*, 621, A26
 Portillo, S. K. N., Parejko, J. K., Vergara, J. R., & Connolly, A. J. 2020, *AJ*, 160, 45
 Roelfsema, P. R., & Allen, R. J. 1985, *A&A*, 146, 213
 Romanishin, W. 1983, *MNRAS*, 204, 909
 Rubin, V. C. 1980, *Mercu*, 9, 78
 Rubin, V. C., Ford, W. K., Jr., & Thonnard, N. 1980, *ApJ*, 238, 471
 Saburova, A., Chilingarian, I., Kasparova, A., et al. 2021, *MNRAS*, 503, 830
 Shallue, C. J., & Vanderburg, A. 2018, *AJ*, 155, 94
 Smith, M. J., Arora, N., Stone, C., Courteau, S., & Geach, J. E. 2021, *MNRAS*, 503, 96
 Vafaei Sadr, A., Bassett, B. A., Oozeer, N., Fantaye, Y., & Finlay, C. 2020, *MNRAS*, 499, 379
 Villar, V. A., Hosseinzadeh, G., Berger, E., et al. 2020, *ApJ*, 905, 94
 Wiegert, T., & English, J. 2014, *NewA*, 26, 40
 Wu, J. F., & Boada, S. 2019, *MNRAS*, 484, 4683
 Wu, J. F., & Peek, J. E. G. 2020, arXiv:2009.12318
 Xu, D., Offner, S. S. R., Gutermuth, R., & Oort, C. V. 2020, *ApJ*, 890, 64